Cancer Research

Dicer1 Phosphomimetic Promotes Tumor Progression and Dissemination

Neeraj K. Aryal[1,2], Vinod Pant[1], Amanda R. Wasylishen[1], Bobbie J. Rimel[3], Laura Baseler[4], Adel K. El-Naggar[5], David G. Mutch[6], Paul J. Goodfellow[7], Swathi Arur[1,2], and Guillermina Lozano[1,2]

Abstract

Dicer1 functions as a tumor suppressor in mouse models. In humans, somatic mutations are associated with many cancers in adults, and patients with DICER1 syndrome with *DICER1* germline mutations are susceptible to childhood cancers. Dicer is phosphorylated by the ERK-MAP kinase pathway and because this pathway is activated in human cancers, we asked whether phosphorylated Dicer1 contributed to tumor development. In human endometrioid cancers, we discovered that phosphorylated DICER1 is significantly associated with invasive disease. To test a direct involvement of Dicer1 phosphorylation in tumor development, we studied mice with phosphomimetic alterations at the two conserved serines phosphorylated by ERK and discovered that a phosphomimetic Dicer1 drives tumor development and dissemination in two independent murine cancer models ($KRas^{+/LA1}$ and $p53^{+/-}$). Our findings demonstrate that phosphomimetic Dicer1 promotes tumor development and invasion.

Significance: This work highlights the relevance of Dicer1 phosphorylation in mammalian tumor development and dissemination.

Introduction

DICER1 is an essential ribo-endonuclease that processes pre-miRNAs into functional miRNAs (1–3). *DICER1* acts as a haploinsufficient tumor suppressor: somatic heterozygous mutations are frequently observed in human cancers and heterozygosity promotes tumorigenesis in several murine tumor models (4–8). Patients with DICER1 syndrome carry germline heterozygous mutations in *DICER1* (missense and truncating), and have increased risk for a variety of cancers including pleuropulmonary blastoma, ovarian sex cord stromal tumors, cystic nephroma, and thyroid cancer (8–10).

Dicer (DCR-1) is phosphorylated by ERK in the KRAS signaling axis in *Caenorhabditis elegans* (11). In this context, phosphorylated Dicer is nuclear and drives the oocyte to embryo transition, indicating a novel role for Dicer during this key reprogramming event in development (11). The phosphorylation sites (serines 1712 and 1836 in mice, and serines 1728 and 1852 in humans) and the nuclear localization of phospho-Dicer1 are well conserved in murine and human cells (11). Using phospho-specific antibodies to cognate residues in human DICER1, we found that DICER1 was phosphorylated in response to fibroblast growth factor activation in cultured human cells (11). We, therefore, examined a role for Dicer1 phosphorylation in tumor development by assaying human primary endometrioid tumors and by evaluating tumorigenesis in a phosphomimetic *Dicer1* knock-in mouse model wherein serines 1712 and 1836 were replaced with aspartic acids. We discovered that (i) phosphorylated DICER1 is present in majority of endometrioid cancers, and is significantly associated with invasive disease and (ii) phosphomimetic Dicer1 drives tumor development and dissemination in two independent murine cancer models ($KRas^{+/LA1}$ and $p53^{+/-}$). Our findings implicate phosphorylated Dicer1 in tumor development.

Materials and Methods

IHC of human tumors

IHC was performed on a tumor microarray (TMA) of 54 primary endometrioid cancer cases. These are untreated tumor samples. Four separate cores were obtained from areas of viable tumor tissue in paraffin blocks of formalin-fixed tumors. The areas for inclusion in the TMA were determined by a gynecologic pathologist. The TMA was then created as described previously (12). Practical methods for TMA construction has been described previously (12). Five-micrometer sections of the TMA block were obtained and stained for anti–phospho-DICER1 and anti–phospho-ERK mAbs. Anti–phospho-DICER1 mAbs were generated in house and tested for specificity as previously described (11). Phospho-ERK staining was performed with

[1]Department of Genetics, The University of Texas MD Anderson Cancer Center, Houston, Texas. [2]Genes and Development Program, The University of Texas MD Anderson Cancer Center UTHealth Graduate School of Biomedical Sciences, Houston, Texas. [3]Division of Gynecologic Oncology, Cedars Sinai Medical Center, Los Angeles, California. [4]Department of Veterinary Medicine and Surgery, The University of Texas MD Anderson Cancer Center, Houston, Texas. [5]Department of Pathology, The University of Texas MD Anderson Cancer Center, Houston, Texas. [6]Department of Obstetrics and Gynecology, Division of Gynecologic Oncology, Washington University School of Medicine and Siteman Cancer Center, St. Louis, Missouri. [7]Department of Obstetrics and Gynecology, Division of Gynecologic Oncology, The Ohio State University and James Comprehensive Cancer Center, Columbus, Ohio.

Note: Supplementary data for this article are available at Cancer Research Online (http://cancerres.aacrjournals.org/).

Corresponding Authors: Guillermina Lozano, The University of Texas MD Anderson Cancer Center, 1515 Holcombe Blvd. Unit 1010, Houston, TX 77030. Phone: 713-834-6386; Fax: 713-834-6380; E-mail: gglozano@mdanderson.org; and Swathi Arur, E-mail: sarur@mdanderson.org

doi: 10.1158/0008-5472.CAN-18-2460

anti–phospho-ERK (Thr 202/Tyr 204, #9101 S, rabbit anti-human, Cell Signaling Technology) at 1:100 dilution. Slides were then incubated MACH2 Universal polymer-HRP (#M2U522H, BioCare Medical, LLC). Signals were developed with the 3,3′-diaminobenzidine (DAB) substrate DAB$^+$ Liquid (#K3468, Dako Cytomation). Slides were read by two blinded independent examiners. Staining for each antibody was reviewed and recorded as a percentage of cells with nuclear stain and a percentage of cells with cytoplasmic stain. The percentages were averaged between examiners.

Mice

KRas^{LA1}, *p53$^-$*, and *Dicer^{2SD}* alleles have been published (13–15). All mice were maintained in >90% C57BL/6 background. All mouse studies were conducted in compliance with an Institutional Animal Care and Use Committee-approved protocol.

We crossed *Dicer$^{+/2SD}$* and *KRas$^{+/LA1}$* mice to generate a cohort of *KRas$^{+/LA1}$* and *KRas$^{+/LA1}$ Dicer$^{+/2SD}$* mice. The cohort was monitored for 400 days. Moribund animals were euthanized, and their tissues were collected. Animals that were still alive at 400 days were sacrificed and their tissues were collected for pathology. Animals that were euthanized due to nontumor related issues (dermatitis, rectal prolapse) were not included in the study.

Similarly, we introduced the *Dicer^{2SD}* allele in the *p53$^{+/-}$*-driven tumor model. A cohort containing 19 *p53$^{+/-}$* mice and 32 *p53$^{+/-}$ Dicer$^{+/2SD}$* mice was generated. The cohort was monitored for 540 days. Moribund animals were euthanized, and their tissues were collected. Animals that were still alive at 540 days were sacrificed and their tissues were collected for pathology. Animals that were euthanized because of nontumor-related issues (dermatitis, rectal prolapse) were not included in the study. Tissues were collected, sectioned, and examined for pathology at the same time.

Histopathology

Tissues harvested from mice were fixed in 10% neutral buffered formalin and paraffin-embedded. Four-micrometer sections were stained with hematoxylin and eosin (H&E), and examined by light microscopy. Tissue processing, paraffin embedding, sectioning, and H&E staining were performed by the MD Anderson Department of Veterinary Medicine & Surgery Histology Laboratory.

Immunofluorescence staining

Tissues were harvested from mice, fixed in 10% neutral buffered formalin, and paraffin-embedded. Tissue processing was performed by the MD Anderson Department of Veterinary Medicine & Surgery Histology Laboratory. Immunofluorescence to detect phosphorylation of Dicer1 was conducted with monoclonal phospho-Dicer1 specific antibodies (clones 1712-26 and 1836-25; 1:200; ref. 11), and DAPI. For each genotype, 50 images at 63× were captured across the full slide. Each image captured 200 to 500 cells. To avoid bias, staining, and image capture, analyses were performed in a blinded manner.

Statistical analysis

Student *t* tests, Fisher exact tests, and Kaplan–Meier survival analyses were performed using GraphPad Prism 7 Software. *P* values were calculated using log-rank (Mantel–Cox) test and $P < 0.05$ was considered statistically significant.

Results

DICER1 phosphorylation correlates with endometrioid tumor invasion

Dicer phosphorylation at serines 1712 and 1836 and nuclear translocation are mediated by Erk downstream of the KRas signaling pathway (11). We, therefore, examined DICER1 phosphorylation status in 54 endometrioid cancers with increased KRAS or hormonal signaling by IHC for phospho-DICER1 and phospho-ERK on a tissue microarray. These 54 endometrioid tumors had an intact DNA mismatch repair (MMR) pathway based on prior microsatellite instability analyses (16). Endometrioid tumors with an intact MMR pathway do not present with *DICER1* mutations. *POLE* mutations also were not identified in these samples (16).

To examine the status of phospho-DICER1 in these tumors, we used two phospho-Dicer1 monoclonal antibodies (mAb) mixed together that recognize individual phosphorylated serines 1728 and 1852. The specificities of these reagents have been validated in *C. elegans*, murine uterine tissues, and human cell lines (11, 17). Tumors were also analyzed for phospho-ERK. Each tumor with >10% of cells with phospho-DICER1 or phospho-ERK signal was labeled positive (Fig. 1). Phosphorylated DICER1 appears nuclear in all our assays as shown previously (Fig. 1; refs. 11, 14). We observed that 63% (32/51) of endometrioid tumors (three cases were not evaluated due to >2 lost cores of 5 examined for each tumor) were positive for phospho-DICER1 (Fig. 1). Overall, 84% of tumors that were positive for phospho-DICER1and also for phospho-ERK (27/32) and five were negative for phospho-ERK (either nuclear or cytoplasmic). Of the 19 tumors that were negative for phospho-DICER1, 12 were also negative for phospho-ERK. The distribution of phospho-DICER1–positive cells did not perfectly overlap with phospho-ERK, which could be an indication of the kinetics of phospho-ERK versus phospho-Dicer turnover due to the presence of different phosphatases. Five tumors that were positive for phospho-Dicer1 were negative for phospho-ERK.

To dissect the relationship between DICER1 phosphorylation and clinicopathologic features in endometrioid cancers, we classified each tumor with less than 50% of cells positive for phospho-DICER1 as "low-to-medium" for DICER1 phosphorylation ($n = 35$), and tumors with over 50% of cells with phospho-DICER1 as "high" for DICER1 phosphorylation ($n = 16$). High phospho-DICER1 was significantly associated with lower body mass index (BMI; $P < 0.01$) and deep myometrial invasion ($P = 0.02$; Fig. 1C; Table 1). In addition, there was also a trend wherein the presence of lymphovascular space invasion was higher in tumors with high phospho-DICER1 ($P = 0.06$). Deep myometrial invasion and increased lymphovascular space invasion are features of poor outcomes in these cancers. Together, these data indicate that presence of nuclear phosphorylated DICER1 correlates with lower BMI and endometrioid tumor invasion.

Phosphomimetic Dicer1 cooperates with *KRas^{G12D}* in transformation

To determine whether phosphorylated Dicer1 could drive tumor progression *in vivo*, we generated a *Dicer1* knock-in mouse model by replacing serines 1712 and 1836 (corresponding to human serines 1728 and 1852) with aspartic acid, which mimics phosphorylation and renders the protein impervious to dephosphorylation by phosphatases (13). Dicer1 serines 1712 and 1836 were replaced with aspartic acids (*Dicer^{2SD}*) at the endogenous

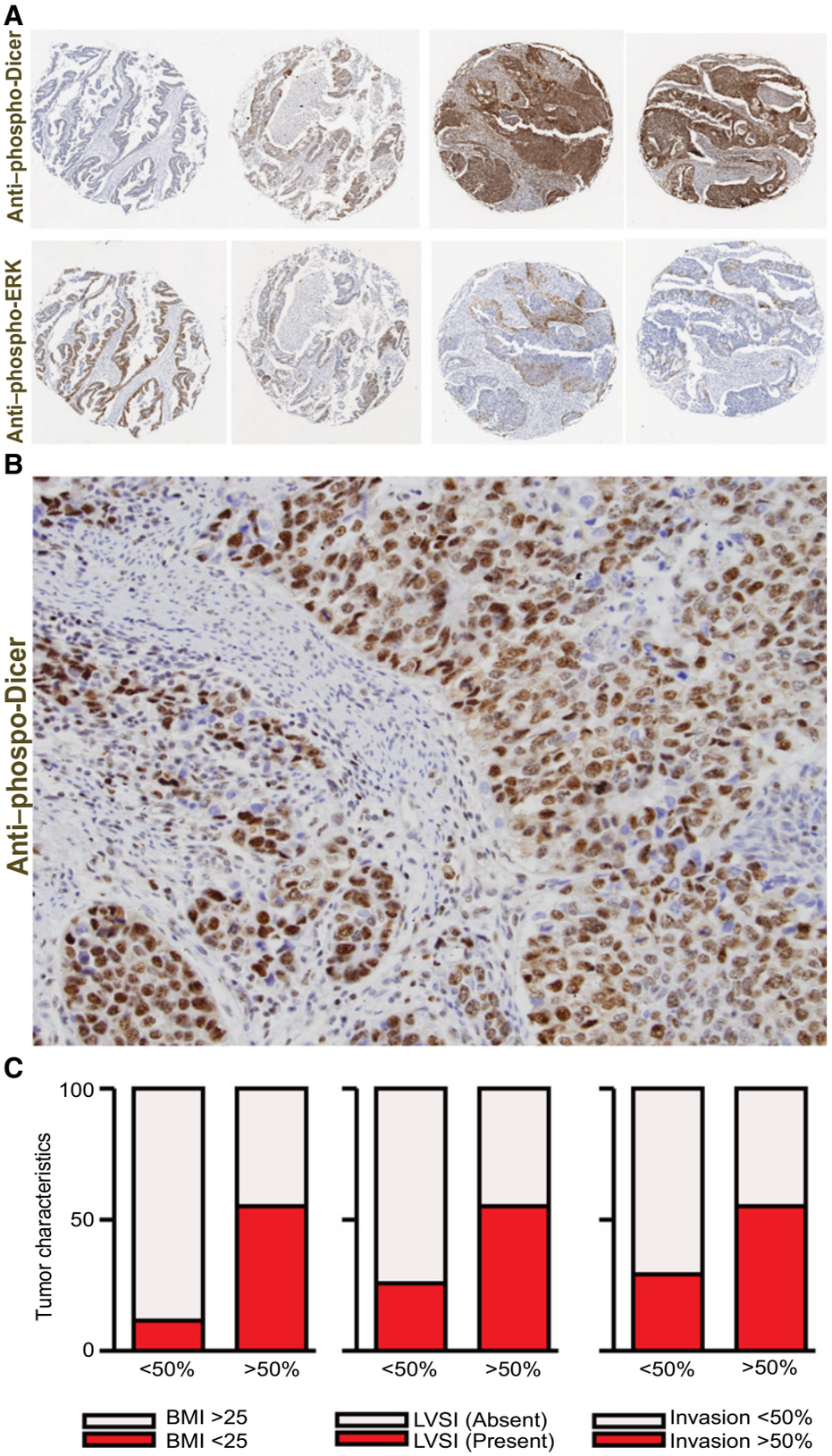

Figure 1.

DICER1 phosphorylation is associated with lower BMI and invasion of primary endometrioid cancers. **A,** Representative images of endometrioid cancers stained with phospho-specific DICER1 antibodies (top) and a phospho-ERK antibody (bottom). **B,** Higher magnification of one endometrioid cancer sample displaying nuclear phosphorylated DICER1 staining. **C,** On the basis of the number of cells that were positive for phospho-DICER1 (**A**), the tumors were divided into "low-to-medium" positivity for phosphorylated DICER1 or "high" positivity for phosphorylated DICER1. Bar graphs display the distribution of tumors with low-to-medium or high phospho-DICER1 with clinicopathologic feature. Invasion, depth of myometrial invasion; LVSI, lymphovascular space invasion. $P < 0.01$ for BMI, $P = 0.06$ for LVSI, and $P = 0.02$ for depth of myometrial invasion.

Table 1. Relationship between phospho-DICER1 levels and clinicopathologic features in endometrioid cancer

Clinicopathologic factor	Nuclear DICER1 positivity			
	Low *N*	Medium *N*	High *N*	*P*[a]
Age				
<60 years	5	10	7	0.10
≥60 years	14	6	9	
BMI				
<25 (Normal or underweight)	2	2	8	<0.01
≥25–30 (Overweight)	16	14	6	
Grade				
1	9	9	9	0.80
2	3	3	1	
3	7	4	6	
Stage				
I or II	12	11	8	0.54
III or IV	7	5	8	
LVSI				
Present	7	2	9	0.03
Absent	12	14	7	
Depth of invasion				
<50%	10	13	5	0.02
≥50%	9	3	11	

NOTE: BMI data missing for three cases.
Abbreviation: LVSI, lymphovascular space invasion.
[a]Fisher exact test.

locus. Homozygosity of Dicer1 phosphomimetic mutations results in highly penetrant postnatal lethality (78%). The few surviving mice are infertile and display accelerated aging phenotypes (13). However, heterozygous mutants are phenotypically normal (13). In light of our observations above that phospho-DICER1 was present in tumors and correlated with invasion, we tested whether phospho-Dicer1 could modulate tumor progression in two independent cancer models. To assess cancer phenotypes independently of developmental lethality displayed by the homozygous mutants, we used heterozygous $Dicer^{2SD}$ mice in two distinct cancer models carrying $KRas^{LA1}$ or $p53^{-}$ mutations (14, 15).

The $KRas^{LA1}$ allele consists of a duplicated exon1, one of which contains a $KRas^{G12D}$ mutation, which undergoes spontaneous recombination yielding either wild-type or mutant *KRas* alleles (15). This model gives rise to fully penetrant multifocal lung cancer starting at 1 week of age and low frequency thymic lymphomas that vary by the background of the mouse. We chose this tumor model because heterozygosity of *Dicer1* cooperates with $KRas^{G12D}$ to drive lung cancer development in mice. We, thus, generated a cohort of $KRas^{+/LA1}$ and $KRas^{+/LA1}$ $Dicer^{+/2SD}$ mice. $KRas^{+/LA1}$ $Dicer^{+/2SD}$ mice contain one phosphomimetic *Dicer1* allele that mimics constitutive phosphorylation and one wild-type *Dicer1* allele that can be potentially regulated by KRas (4). In this background, $KRas^{+/LA1}$ $Dicer^{+/2SD}$ mice developed a wide spectrum of tumors and had a significantly reduced median survival of 353 days as compared with $KRas^{+/LA1}$ mice, which did not achieve median age at the 400-day end point of the study ($P = 0.03$; Fig. 2A). $KRas^{+/LA1}$ mice developed only lung adenomas/adenocarcinomas (16/17). Although $KRas^{+/LA1}$ $Dicer^{+/2SD}$ mice also developed lung adenocarcinomas (21/24), 58% of mice (14/24) developed additional tumors, which included 21% lymphomas (5/24, includes 3 animals without lung adenocarcinoma), 25% histiocytic sarcoma (6/24), and one each of hepatocellular carcinoma, mesothelioma, endothelial cell tumor, hemangiosarcoma, and hemangioma (Fig. 2B and C; Supplementary Fig. S1; Table 2). Of note, all lymphomas and histiocytic sarcomas from $KRas^{+/LA1}$ $Dicer^{+/2SD}$ mice disseminated into multiple organs including lung, liver, heart, kidney, spleen, and thymus (Supplementary Fig. S1; Table 2). In one $KRas^{+/LA1}$; $Dicer^{+/2SD}$ mouse, a lung adenocarcinoma metastasized to the kidney and heart (Supplementary Fig. S1).

To determine whether the phosphomimetic Dicer1 protein behaved as a constitutively phosphorylated protein, we performed immunofluorescence on lung tissues from each of the genotypes using the phospho-Dicer1 antibodies. All $Dicer^{2SD/2SD}$ lung cells were positive for phospho-Dicer1 and all displayed nuclear localization, whereas $Dicer^{+/2SD}$ lung tissues showed little staining likely due to low levels of phosphorylated Dicer1 (Fig. 2D). $KRas^{+/LA1}$ lung tissues showed no staining. In contrast, $KRas^{+/LA1}$; $Dicer^{+/2SD}$ lung sections showed that >70% of cells were positive for nuclear phospho-Dicer1 staining, indicating that increased KRas signaling results in increased phosphorylation and nuclear translocation of wild-type Dicer1 in this model (Fig. 2D). Combined, these results indicate that phosphomimetic Dicer1 is nuclear and cooperates with oncogenic $KRas^{G12D}$, resulting in a wide spectrum of tumors and metastases.

Phosphomimetic Dicer1 cooperates with *p53* heterozygosity in transformation

TP53 loss is associated with *DICER1* mutations and an activated KRAS pathway in many human tumors (4, 9, 18). To test whether the phosphomimetic Dicer1 is sufficient to promote tumorigenesis in the context of *p53* heterozygosity, we next introduced the $Dicer^{2SD}$ allele into $p53^{+/-}$ mice, which primarily developed osteosarcomas and lymphomas (14). Similar to the $KRas^{+/LA1}$ $Dicer^{+/2SD}$ model, $p53^{+/-}$ $Dicer^{+/2SD}$ mice ($n = 32$) exhibited a reduced median survival of 497 days as compared with $p53^{+/-}$ mice ($n = 19$), which did not achieve median age at the 540-day end point used in this study ($P = 0.0855$, Fig. 3A). In addition, $p53^{+/-}$ $Dicer^{+/2SD}$ mice exhibited a wide spectrum of tumors and had a significantly reduced tumor-free survival as compared with $p53^{+/-}$ mice ($P = 0.0273$, Fig. 3B). A total of 71% (15/21) of the $p53^{+/-}$ $Dicer^{+/2SD}$ mice developed tumors as compared with 25% (3/12) of the $p53^{+/-}$ mice (Table 3). In contrast to $p53^{+/-}$ mice, which only developed osteosarcomas ($n = 2$) and a lymphoma ($n = 1$), the spectrum of tumors in $p53^{+/-}$ $Dicer^{+/2SD}$ mice included osteosarcomas ($n = 6$), lymphomas ($n = 6$), histiocytic sarcomas ($n = 2$), hemangiosarcoma, lung adenocarcinoma, hepatocellular carcinoma, testicular carcinoma, and two undifferentiated tumors. A total of 24% of $p53^{+/-}$ $Dicer^{+/2SD}$ mice (5/24) displayed multiple cancers including one mouse that developed an osteosarcoma, a lymphoma, and an adenocarcinoma (Fig. 3C and D; Table 3). Interestingly, lymphomas, histiocytic sarcomas, and the testicular carcinoma were disseminated to many organs, a phenotype also observed in $KRas^{+/LA1}$ $Dicer^{+/2SD}$ mice (Fig. 3D; Table 3). None of the $p53^{+/-}$ mice developed multiple cancers.

We next performed immunofluorescence to assess the status of Dicer1 phosphorylation in $p53^{+/-}$ $Dicer^{+/2SD}$ tumors. We could not detect a signal in $p53^{+/-}$ tumors (Fig. 3E). In contrast, $p53^{+/-}$ $Dicer^{+/2SD}$ lymphomas and osteosarcomas revealed over 60% of cells with positive phospho-Dicer1 nuclear signal. In this genotype, we also evidenced some cytoplasmic signal for the antibody, which may be an indication of cytoplasmic retention of the phosphorylated protein. These results demonstrate that phosphomimetic Dicer is nuclear in tumors from $p53^{+/-}$ mice.

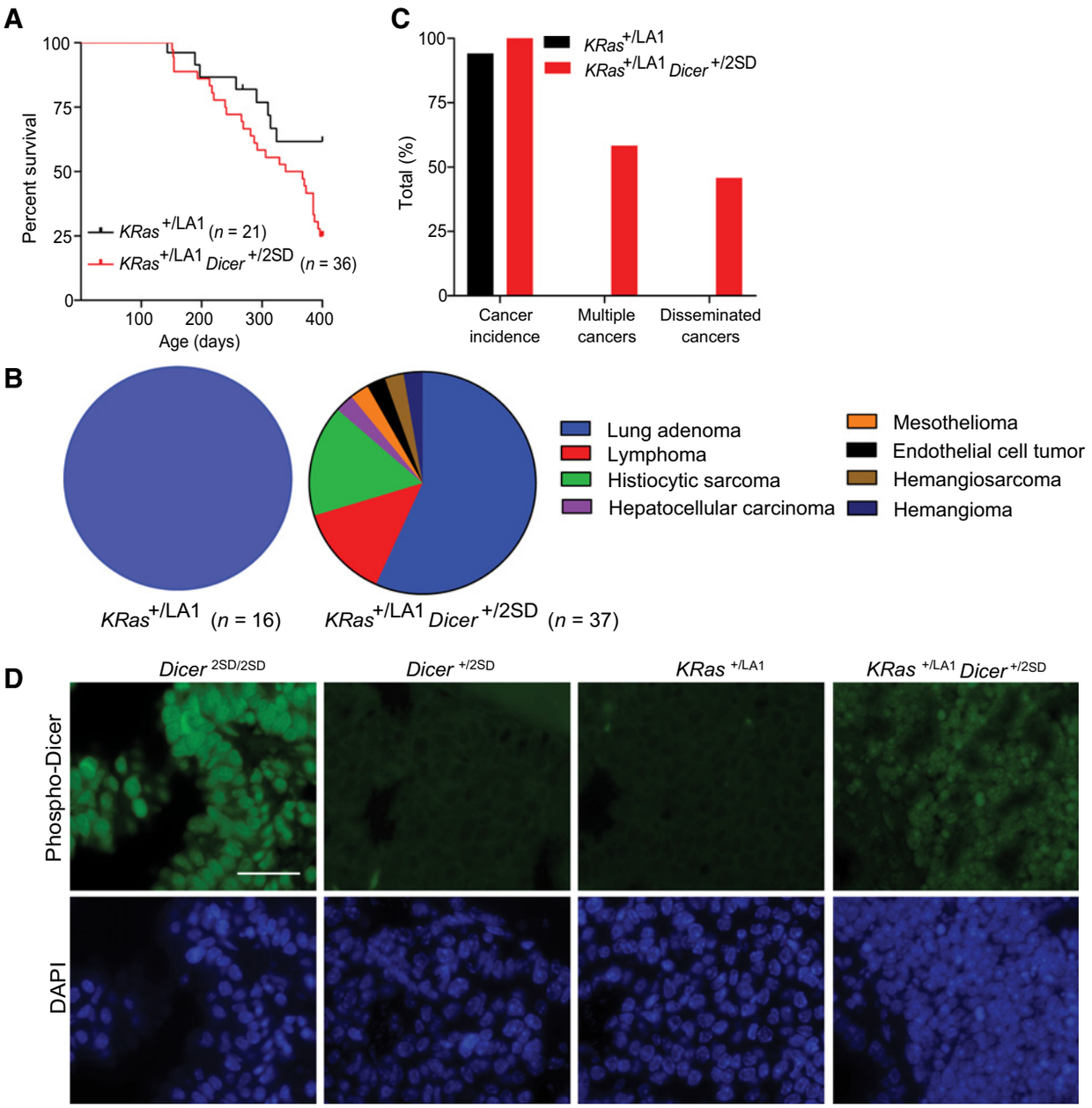

Figure 2.

Phosphomimetic Dicer1 promotes tumorigenesis in $KRas^{+/LA1}$ mice. **A,** Kaplan–Meier survival curves of $KRas^{+/LA1}$ mice ($n = 21$) and $KRas^{+/LA1}$ $Dicer^{+/2SD}$ mice ($n = 36$) followed for 400 days. $P = 0.03$. **B,** Tumor spectrum of $KRas^{+/LA1}$ mice ($n = 16$ cancers in 17 mice) and $KRas^{+/LA1}$ $Dicer^{+/2SD}$ mice ($n = 37$ cancers in 24 mice). **C,** Frequencies of mice with cancer, multiple cancers, and disseminated cancers in $KRas^{+/LA1}$ mice ($n = 17$) and $KRas^{+/LA1}$ $Dicer^{+/2SD}$ mice ($n = 24$). **D,** Representative immunofluorescence images of lung tissue captured at 63× displaying phosphorylated Dicer1 in green and DAPI in blue, in mice with the indicated genotypes. Scale bar, 50 μm.

Combined, these data suggest that phosphomimetic Dicer1 is a key driver of tumor progression and dissemination.

Discussion

Dicer1 is phosphorylated by ERK upstream of KRas, a well-known and studied oncogene. We show for the first time that phospho-Dicer1 is present in endometrioid cancers, localized to the nucleus, and is correlated with invasive disease. In this study, the phosphorylation status of Dicer1 and ERK did not completely overlap. Five tumors that were positive for phospho-Dicer1 were negative for phospho-ERK. This observation suggests that either DICER1 may be phosphorylated by additional MAPK's or that the perdurance of DICER1 phosphorylation is longer than that of phospho-ERK. This observation highlights lack of knowledge regarding the complete regulation

Table 2. Tumors in *KRas*$^{+/LA1}$ and *KRas*$^{+/LA1}$ *Dicer*$^{+/2SD}$ mice

Tumor type	KRas$^{+/LA1}$ ($n = 17$)	KRas$^{+/LA1}$ Dicer$^{+/2SD}$ ($n = 24$)
Lung adenocarcinoma		
	16	21(1[a])
Other tumors		
Lymphoma	0	5(5[a])
Histiocytic sarcoma	0	6(6[a])
Hepatocellular carcinoma	0	1
Mesothelioma	0	1
Endothelial cell tumor	0	1
Hemangiosarcoma	0	1
Hemangioma	0	1
Mice with >1 tumor types	0	14
Total mice with tumors	16	24

[a]Dissemination/metastasis.

of Dicer1 phosphorylation and possible unique functions in the nucleus.

On the basis of these data, the role of the Dicer1 phosphomimetic protein in tumorigenesis was examined in this study. We demonstrate, for the first time, that phosphomimetic Dicer1 cooperates with two distinct oncogenic lesions, *KRas*^{LA1} and *p53*$^{-}$, to drive tumorigenesis, a diverse tumor spectrum, and dissemination. In addition, the development of multiple cancers in a high percentage of mice in both models indicates that phosphomimetic Dicer1 not only plays a role in tumor development and dissemination, but also sensitizes multiple cell types for tumor development. Finally, these observations in mice coupled with the correlation between phospho-DICER1 and invasive endometrioid cancer in humans indicate that Dicer1 phosphorylation promotes tumor invasion and metastasis. Additional data are needed to determine whether phosphorylated DICER1

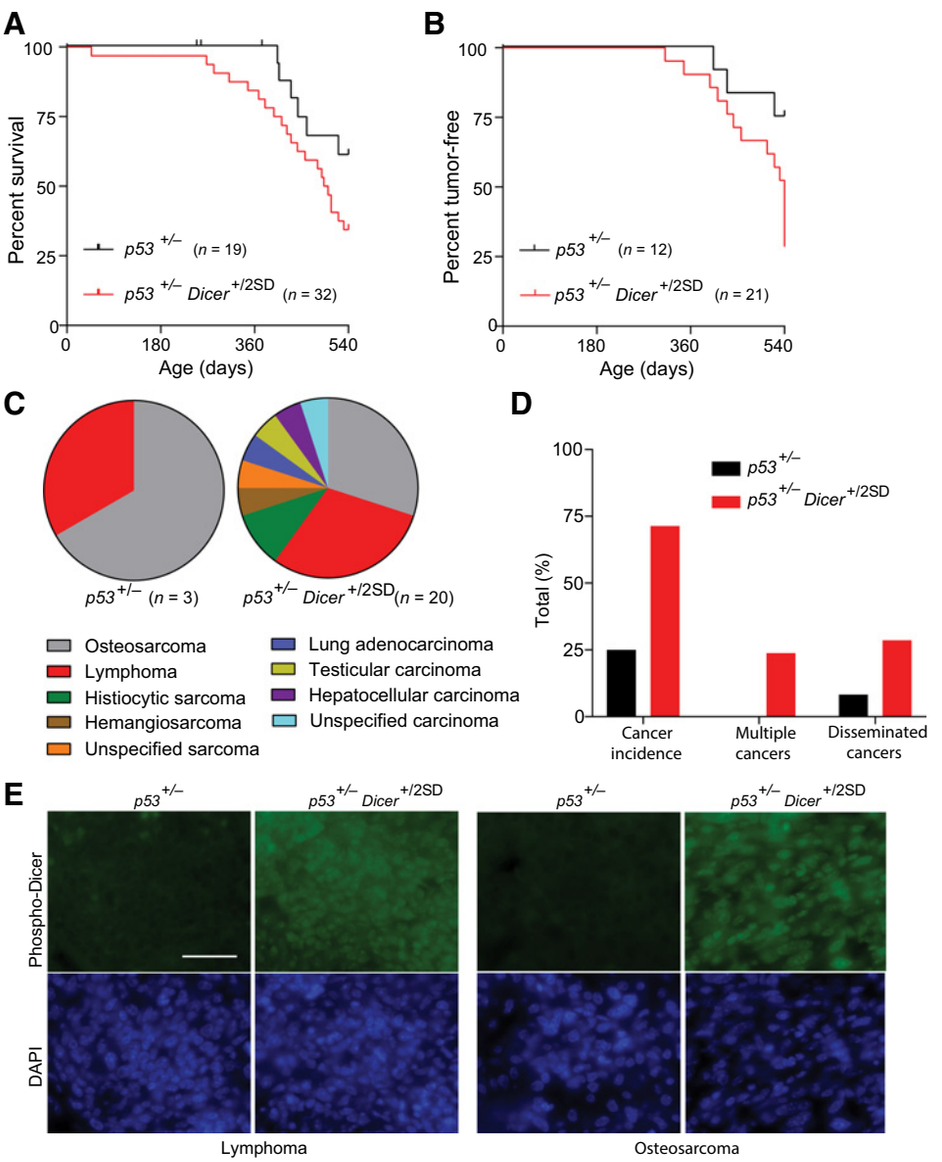

Figure 3.

Phosphomimetic Dicer1 promotes tumorigenesis in *p53*$^{+/-}$ mice. **A,** Kaplan–Meier survival curve of *p53*$^{+/-}$ mice ($n = 19$) and *p53*$^{+/-}$ *Dicer*$^{+/2SD}$ mice ($n = 32$) followed for 540 days. $P = 0.0855$. **B,** Kaplan–Meier survival analysis of tumor-free survival of *p53*$^{+/-}$ mice ($n = 12$) and *p53*$^{+/-}$ *Dicer*$^{+/2SD}$ mice ($n = 21$) followed for 540 days. $P = 0.0273$. **C,** Tumor spectrum of *p53*$^{+/-}$ mice ($n = 3$ cancers in 12 mice) and *p53*$^{+/-}$ *Dicer*$^{+/2SD}$ mice ($n = 20$ cancers in 21 mice). **D,** Frequencies of mice with cancer, multiple cancers, and disseminated cancers in *p53*$^{+/-}$ mice ($n = 12$) and *p53*$^{+/-}$ *Dicer*$^{+/2SD}$ mice ($n = 21$). **E,** Representative immunofluorescence images of lymphomas and osteosarcomas captured at 63× displaying phosphorylated Dicer in green and DAPI in blue, in mice of the indicated genotypes. Scale bar, 50 μm.

Table 3. Tumors in $p53^{+/-}$ mice and $p53^{+/-}$ $Dicer^{+/2SD}$ mice

Tumor type	$p53^{+/-}$ ($n = 12$)	$p53^{+/-}$ $Dicer^{+/2SD}$ ($n = 21$)
Sarcoma		
Ostersarcoma	2	6
Histiocytic sarcoma	0	2(2[a])
Hemangiosarcoma	0	1
Unspecified	0	1
Lymphoma		
	1(1[a])	6(3[a])
Carcinoma		
Lung adenocarcinoma	0	1
Testicular carcinoma	0	1(1[a])
Hepatocellular carcinoma	0	1
Unspecified	0	1
Mice with >1 tumor type	0	5
Total mice with tumors	3	15

[a]Dissemination/metastasis.

contributes to a broader spectrum of human cancers. Our discovery highlights a need to further investigate DICER1 phosphorylation status as an indicator of tumor progression and dissemination in human cancers.

Disclosure of Potential Conflicts of Interest

D.G. Mutch has received speakers bureau honoraria form Clovis. No potential conflicts of interest were disclosed by the other authors.

Authors' Contributions

Conception and design: N.K. Aryal, D.G. Mutch, S. Arur, G. Lozano
Development of methodology: N.K. Aryal, B. Rimel, D.G. Mutch
Acquisition of data (provided animals, acquired and managed patients, provided facilities, etc.): N.K. Aryal, V. Pant, B. Rimel, D.G. Mutch, P.J. Goodfellow
Analysis and interpretation of data (e.g., statistical analysis, biostatistics, computational analysis): N.K. Aryal, A.R. Wasylishen, L. Baseler, A.K. El-Naggar, P.J. Goodfellow, S. Arur, G. Lozano
Writing, review, and/or revision of the manuscript: N.K. Aryal, V. Pant, A.R. Wasylishen, L. Baseler, D.G. Mutch, P.J. Goodfellow, S. Arur, G. Lozano
Administrative, technical, or material support (i.e., reporting or organizing data, constructing databases): N.K. Aryal, V. Pant, A.K. El-Naggar, D.G. Mutch
Study supervision: N.K. Aryal, D.G. Mutch, S. Arur, G. Lozano

Acknowledgments

NIH grants CA82577 to G. Lozano and GMR0198200 to S. Arur partially supported this study. This study is also supported in part by P50CA134254 and P50CA16672. S. Arur is an Andrew Sabin Family Foundation Fellow at The University of Texas MD Anderson Cancer Center. N.K. Aryal is a Gigli Family Endowed Scholar at The University of Texas MD Anderson Cancer Center UTHealth Graduate School of Biomedical Sciences.

The costs of publication of this article were defrayed in part by the payment of page charges. This article must therefore be hereby marked *advertisement* in accordance with 18 U.S.C. Section 1734 solely to indicate this fact.

Received August 8, 2018; revised October 23, 2018; accepted March 22, 2019; published first March 26, 2019.

References

1. Bernstein E, Kim SY, Carmell MA, Murchison EP, Alcorn H, Li MZ, et al. Dicer is essential for mouse development. Nat Genet 2003;35:215–7.
2. Yang WJ, Yang DD, Na S, Sandusky GE, Zhang Q, Zhao G. Dicer is required for embryonic angiogenesis during mouse development. J Biol Chem 2005;280:9330–5.
3. Nicholson RH, Nicholson AW. Molecular characterization of a mouse cDNA encoding Dicer, a ribonuclease III ortholog involved in RNA interference. Mamm Genome 2002;13:67–73.
4. Kumar MS, Pester RE, Chen CY, Lane K, Chin C, Lu J, et al. Dicer1 functions as a haploinsufficient tumor suppressor. Genes Dev 2009;23:2700–4.
5. Yoshikawa T, Otsuka M, Kishikawa T, Takata A, Ohno M, Shibata C, et al. Unique haploinsufficient role of the microRNA-processing molecule Dicer1 in a murine colitis-associated tumorigenesis model. PLoS One 2013;8:e71969.
6. Lambertz I, Nittner D, Mestdagh P, Denecker G, Vandesompele J, Dyer MA, et al. Monoallelic but not biallelic loss of Dicer1 promotes tumorigenesis *in vivo*. Cell Death Differ 2010;17:633–41.
7. Arrate MP, Vincent T, Odvody J, Kar R, Jones SN, Eischen CM. MicroRNA biogenesis is required for Myc-induced B-cell lymphoma development and survival. Cancer Res 2010;70:6083–92.
8. Foulkes WD, Priest JR, Duchaine TF. DICER1: mutations, microRNAs and mechanisms. Nat Rev Cancer 2014;14:662–72.
9. Pugh TJ, Yu W, Yang J, Field AL, Ambrogio L, Carter SL, et al. Exome sequencing of pleuropulmonary blastoma reveals frequent biallelic loss of TP53 and two hits in DICER1 resulting in retention of 5p-derived miRNA hairpin loop sequences. Oncogene 2014;33:5295–302.
10. Klein S, Lee H, Ghahremani S, Kempert P, Ischander M, Teitell MA, et al. Expanding the phenotype of mutations in DICER1: mosaic missense mutations in the RNase IIIb domain of DICER1 cause GLOW syndrome. J Med Genet 2014;51:294–302.
11. Drake M, Furuta T, Suen KM, Gonzalez G, Liu B, Kalia A, et al. A requirement for ERK-dependent Dicer phosphorylation in coordinating oocyte-to-embryo transition in C. elegans. Dev Cell 2014;31:614–28.
12. Fedor HL, De Marzo AM. Practical methods for tissue microarray construction. Methods Mol Med 2005;103:89–101.
13. Aryal NK, Pant V, Wasylishen AR, Parker-Thornburg J, Baseler L, El-Naggar AK, et al. Constitutive Dicer1 phosphorylation accelerates metabolism and aging in vivo. Proc Natl Acad Sci U S A 2018;116:960–9.
14. Jacks T, Remington L, Williams BO, Schmitt EM, Halachmi S, Bronson RT, et al. Tumor spectrum analysis in p53-mutant mice. Curr Biol 1994;4:1–7.
15. Johnson L, Mercer K, Greenbaum D, Bronson RT, Crowley D, Tuveson DA, et al. Somatic activation of the K-ras oncogene causes early onset lung cancer in mice. Nature 2001;410:1111–6.
16. Billingsley CC, Cohn DE, Mutch DG, Stephens JA, Suarez AA, Goodfellow PJ. Polymerase varepsilon (POLE) mutations in endometrial cancer: clinical outcomes and implications for Lynch syndrome testing. Cancer 2015;121:386–94.
17. Burger K, Schlackow M, Potts M, Hester S, Mohammed S, Gullerova M. Nuclear phosphorylated Dicer processes double-stranded RNA in response to DNA damage. J Cell Biol 2017;216:2373–89.
18. Rakheja D, Chen KS, Liu Y, Shukla AA, Schmid V, Chang TC, et al. Somatic mutations in DROSHA and DICER1 impair microRNA biogenesis through distinct mechanisms in Wilms tumours. Nat Commun 2014;2:4802.